J Neurophysiol 101: 2995–3011, 2009.
First published March 25, 2009; doi:10.1152/jn.90740.2008.

Excitatory Actions of Ventral Root Stimulation During Network Activity Generated by the Disinhibited Neonatal Mouse Spinal Cord

Agnes Bonnot, Nikolai Chub, Avinash Pujala, and Michael J. O'Donovan
Developmental Neurobiology Section, National Institute of Neurological Disorders and Stroke, National Institutes of Health, Bethesda, Maryland

Submitted 7 July 2008; accepted in final form 23 March 2009

Bonnot A, Chub N, Pujala A, O'Donovan MJ. Excitatory actions of ventral root stimulation during network activity generated by the disinhibited neonatal mouse spinal cord. *J Neurophysiol* 101: 2995–3011, 2009. First published March 25, 2009; doi:10.1152/jn.90740.2008. To further understand the excitatory effects of motoneurons on spinal network function, we investigated the entrainment of disinhibited rhythms by ventral root (VR) stimulation in the neonatal mouse spinal cord. A brief train of stimuli applied to a VR triggered bursting reliably in 31/32 experiments. The same roots that entrained disinhibited bursting could also produce locomotor-like activity with a similar probability when the network was not disinhibited. The ability of VR stimulation to entrain the rhythm persisted in nicotinic and muscarinic cholinergic antagonists but was blocked by the AMPAR antagonist NBQX. Bath application of the type I mGluR1 receptor antagonist CPCCOEt reduced the ability of both dorsal root and VR stimulation to entrain the disinhibited rhythm and abolished the ability of either type of stimulation to evoke locomotor-like activity. Calcium imaging through the lateral aspect of the cord revealed that VR stimulation and spontaneously occurring bursts were accompanied by a wave of activity that originated ventrally and propagated dorsally. Imaging the cut transverse face of L_5 revealed that the earliest VR-evoked optical activity began ventrolaterally. The optical activity accompanying spontaneous bursts could originate ventrolaterally, ventromedially, or throughout the mediolateral extent of the ventral horn or very occasionally dorsally. Collectively, our data indicate that VR stimulation can entrain disinhibited spinal network activity and trigger locomotor-like activity through a mechanism dependent on activation of both ionotropic and metabotropic glutamate receptors. The effects of entrainment appear to be mediated by a ventrolaterally located network that is also active during spontaneously occurring bursts.

INTRODUCTION

Mammalian motoneurons are generally assumed to be the output elements of the mammalian spinal cord that do not contribute causally to the genesis of locomotion or to other motor behaviors. This view arose because the only known functional projections of motoneurons are to Renshaw cells, which are inhibitory. However, in the tadpole, motoneurons make synaptic connections with each other and with interneurons belonging to the central pattern generator for swimming (Perrins and Roberts 1995). Moreover, in the chick embryo, rhythmic activity can be triggered by antidromic stimulation of the ventral roots (Wenner and O'Donovan 1999), and motoneurons appear to be the first spinal neurons to become active at the onset of spontaneous episodes and during each subsequent cycle of activity (Arai et al. 2007; Wenner and O'Donovan 2001). In the neonatal mouse, stimulation of motoneuron axons can trigger locomotor-like activity, raising the possibility that motoneuron axons may have access to interneurons projecting to, or even belonging to, the central pattern generator for locomotion (Mentis et al. 2005). The idea that motoneurons might project to spinal neurons other than Renshaw cells has been supported by recent work showing that stimulation of motor axons can excite other motoneurons (Jiang et al. 1991; Machacek and Hochman 2006; Nishimaru et al. 2005) particularly in the presence of exogenously applied noradrenaline (Machacek and Hochman 2006) and can entrain disinhibited bursting (Machacek and Hochman 2006).

The goal of the present work was to investigate further the excitatory actions of ventral root stimulation on the disinhibited bursting produced by the spinal cord in the presence of GABA- and glycinergic antagonists. We chose this approach for several reasons. First, it eliminates the possibility that some of the excitatory actions of ventral root stimulation reported earlier (Mentis et al. 2005) might be mediated by activation of Renshaw cells. Although Renshaw cells are known to be inhibitory in the adult spinal cord, during development, the inhibitory neurotransmitters GABA and glycine can be depolarizing. Second, in the presence of inhibitory antagonists, spinal networks are hyperexcitable which should facilitate the detection of excitatory pathways from motoneurons. Finally we wanted to exploit this hyperexcitability to maximize the optical signals generated in spinal neurons during the evoked or spontaneous synchronized bursting exhibited by the disinhibited cord to establish the timing of motoneuron recruitment with that of other spinal neurons.

In addition to the experimental reasons for examining disinhibited networks, an investigation of the excitatory actions of motoneurons in disinhibited networks may provide some insights into the role of motoneurons during locomotion. It is believed that the networks responsible for disinhibited bursting are located in the ventral part of the cord as is the central pattern generator for locomotion (Bracci et al. 1996a; Kjaerulff and Kiehn 1996). Furthermore, both types of network exhibit a similar sensitivity to block of either class of ionotropic glutamate receptors (Beato et al. 1997; Bracci et al. 1996b; Kjaerulff and Kiehn 1996) and both rhythms are susceptible to modulation by sensory afferent inputs (Bracci et al. 1997). In addition, several studies investigating the interaction between disinhibited bursting and fictive locomotor patterns suggest that some of the same elements might be common to both networks (Beato and Nistri 1999; Cowley and Schmidt 1995; Juvin et al. 2005).

Address for reprint requests and other correspondence: Michael J. O'Donovan, Room 3C-1014 Building 35, 35 Convent Drive, NINDS, NIH, Bethesda, MD 20892 (E-mail: odonovm@ninds.nih.gov).

METHODS

Surgical procedures

Experiments were performed on Swiss Webster neonatal mice (Taconic Laboratory; P2–P3). The mice were either anesthetized with methoxyflurane and then decapitated or decapitated and eviscerated. The remaining tissue was placed in a dissecting chamber and continuously perfused with an artificial cerebrospinal fluid (ACSF; concentrations in mM: 128 NaCl, 4 KCl, 1.5 $CaCl_2$, 1 $MgSO_4$, 0.5 NaH_2PO_4, 21 $NaHCO_3$, 30 D-glucose) bubbled with 95% O_2-5% CO_2. A ventral laminectomy exposed the cord, which was then transected between T_5 and T_7 and removed from the vertebral column together with the attached roots and the cauda equina. The ACSF was initially at a temperature of ~17°C and was progressively warmed to 23–25°C before transfer of the cord to the recording chamber. In some experiments, the ACSF in the dissecting chamber was maintained at ~7–9°C.

Electroporation

Electroporation was carried out as described previously (Bonnot et al. 2005). The isolated spinal cord was pinned down with the ventral side up, and a broken sharp glass electrode was used to pressure-apply 1 μl of calcium-sensitive dye solution under the dura matter, usually at the level of the ventral commissure. A cell-impermeant dye, either Calcium Green-1 dextran 3000MW (25 mM) or Calcium Green-1 hexapotassium salt (55 mM; Molecular Probes, Eugene, OR), was dissolved in the ACSF before application. Two gold-plated electrodes (BTX, rectangular 3 × 5 mm genepaddles) were immediately submerged in the ACSF and positioned in parallel on either side of the lumbosacral cord with a 3-mm interelectrode distance. To minimize the discrepancy between the applied and effective voltages, the level of fluid in the chamber was kept as low as possible at the time of the electroporation. Square voltage pulses (18–24 V, 75-ms duration, 5 pulses at 1 Hz) were applied between the electrodes within 5–10 min after dye application using the ECM 830 electroporation system (BTX). The dura mater was peeled off from the lateral sides in the electroporated area to optimize the visualization of the labeled neurons. The cord was left for ~1 h to allow both washout of the excess of dye from the extracellular space and physiological recovery from electroporation. The cord was then transferred to the recording chamber. In some of the experiments, a low-Ca^{2+}/high-Mg^{2+} ACSF, [concentrations (in mM): 128 NaCl, 4 KCl, 0.1 $CaCl_2$, 5 $MgSO_4$, 0.5 NaH_2PO_4, 21 $NaHCO_3$, 30 D-glucose] was used during dissection and electroporation.

Neuroanatomy

At the end of the experiment, some electroporated preparations were fixed in 1-ethyl-3-(dimethylaminopropyl) carbodiimide hydrochloride (EDC; Sigma-Aldrich, St. Louis, MO) as described previously (Bonnot et al. 2002, 2005). In some cases, ventral roots of the electroporated area were retrogradely labeled with Texas red to identify motoneurons. Preparations were cut in the coronal or parasagittal plane using a vibratome and stacks of images were obtained with a confocal microscope (Olympus FV 300).

Electrophysiology

Motoneuron electrical activity was recorded with tight-fitting plastic suction electrodes into which individual ventral roots were drawn. The recorded signals were filtered (DC-3 kHz), digitized at 10 kHz (NeuroData) and recorded on videotape or alternatively digitized at 10 kHz (Digidata 1322A) and stored on a computer.

In some experiments, the activity of ventrolateral and/or ventromedial white matter funiculi (VLF and/or VMF) was also recorded. Synchronization of the electrical and optical signals was achieved by gating the camera off (which blanked some frames) and recording the gating pulse together with the electrical recordings. Episodes of data were acquired off-line using Clampex and analyzed with Clampfit, Excel, and Matlab. Spinal motoneurons were activated antidromically by square-wave stimulation of the ventral roots (stimulus duration: 200 μs, trains: 5–50 Hz, stimulus intensity: 50–80 μA, train duration: 2 s). Mono- and polysynaptic reflex responses recorded from ventral roots within the electroporated area were evoked by a single electrical stimulus to the homonymous lumbar dorsal root (stimulus duration: 200 μs, stimulus intensity: 18–50 μA). Continuous rhythmic activity was induced by bath application of bicuculline (20–50 μM) and strychnine (1–5 μM), and several ventral roots were stimulated to entrain the induced rhythm. We generally used five pulses at 20 Hz, stimulus intensity: 50–80 μA and stimulus duration: 200 μs because those parameters ensured reliable entrainment in each experiment. The threshold for each of those stimulus parameters (tuned separately while all other parameters were kept unchanged) were, respectively, three pulses, 2 Hz, 18 μA, and 50 μs.

We also investigated the effects of several drugs on the spontaneous and ventral root and dorsal root-evoked activity. These included: the cholinergic antagonists (50 μM mecamylamine, 50 μM dihydro-β-erythroidine, and 5 μM atropine), an *N*-methyl-D-aspartate (NMDA) antagonist (AP5; 50–100 μM), a non-NMDA antagonist 2,3-Dihydroxy-6-nitro-7-sulphamoylbenzo(f)-quinoxaline-2,3-dione (NBQX; 2.5 μM), a selective blocker of AMPA receptor desensitization (cyclothiazide; 25 μM), the mGluR1 antagonist 7-(hydroxyimino)cyclopropa[β]chromen-1α-carboxylate ethyl ester (CPCCOEt, 80 μM) and the mGluR5 antagonist 2-methyl-6-(phenylethynyl)pyridine hydrochloride (MPEP, 25–50 μM).

To quantify the effects of the drugs, we measured several features of the spontaneous and evoked bursting. These included: the cycle period and the burst duration of the spontaneous and evoked bursts; the delay between the last stimulus of each train and the onset of the burst on the ipsilateral ventral root the closest to the stimulated ventral root; the increase of the delay with successive stimuli which was defined as the slope of the delays versus stimulus number plot. Data are expressed as means and ± SE. Statistical differences between experimental and control conditions were measured using *t*-test after assessing the variance with an *F*-test.

Optical imaging

We imaged calcium transients accompanying spontaneous and evoked bursts using two methods. In the first, the cord was placed in a perfusion chamber with a coverslip as its base. The chamber was mounted on an inverted epifluorescence microscope (Nikon Eclipse TE300) and continuously perfused with ACSF. The tissue was illuminated with a 75-W Xenon light source (excitation filter: 470–490 nm, emission filter: 520–560 nm) and viewed through the lateral white matter. Activity-dependent changes in fluorescence were detected using an intensified CCD camera (Stanford Photonics) and stored on videotape (SONY SVO 9500MD). Changes in fluorescence were monitored on-line using a PC-based frame grabber (Matrox Image LC/Flashbus) and image processing software (Metamorph: Universal Imaging). Stacks of images (30 frame/s) that were recorded during stimulated or spontaneous activity were subsequently transferred from the video-tape to the frame grabber for storage and processing.

Quantification of the spread of optical activity was accomplished by measuring the calcium transients in six rectangular regions of interest spanning the ventrodorsal extent of the lateral surface. Measurements were made at 30 frame/s and linear interpolation was used between the individual points. The six transients from several bursts were normalized and then averaged. The onset of the transient was defined as the time the transient crossed a line 2 SD above the mean level of fluorescence before the onset of the burst. The time to reach 50% of the peak signal was also calculated.

We also visualized the calcium transients from the transverse face of the cut spinal cord. To achieve this, the spinal cord was transected between lumbar segments L_5–L_6 and comprised 12–13 segments (T_{5-6} to L_5). The cut, rostral part was labeled with the calcium-sensitive dye fluo-3 AM (Invitrogen, Carlsbad, CA) by injecting the dye into the cut face at multiple locations (Stosiek et al. 2003; Wilson et al. 2007). The dye solution was pressure applied from a glass micropipette (tip diameter: 2–5 μm) using a Pneumatic Pico Pump (PV 800, World Precision Instruments, Sarasota, FL). The dye solution was freshly prepared on the day of experiment: an aliquot of 50 μg dye was first dissolved in 4.5 μl DMSO with 20% Pluronic-127 (Invitrogen), then 95 μl of DPBS (Invitrogen) was added, and the mixture was sonicated for 30–40 min to yield ~0.5 mM final dye concentration. To minimize damage to the gray matter, the dye solution was repetitively applied using short pressure pulses (1-s duration, $n = 25$) with 2-s interpulse intervals. Pressure was adjusted to 10–20 p.s.i., which resulted in the injection of ~9 nl of dye solution per pulse. Usually, the injection sites (50–100 μm deep) were aligned in two rows 200 μm apart in the dorsoventral direction with 100 μm between the sites. The injected spinal cord was washed for 30–40 min and then was transferred to the recording chamber for optical and electrical recording. An Olympus BW61WI upright epifluorescence microscope equipped with a CoolSnap ES digital camera (Photometrics Tucson, AZ) and MetaMorph 7 imaging software (Molecular Devices, Union City, CA) was used for recording of the calcium transients. Electrical activity was recorded from the L_4 or L_5 ventral roots and the L_5 dorsal root using suction electrodes. The L_5 dorsal and ventral roots were also used for stimulation (A365 Stimulus Isolator, World Precision Instruments). Electrical activity was recorded and, using DC amplifiers (AI 402, CyberAmp380), digitized (Digidata 1322A) and subsequently analyzed with pClamp 9 software (all from Molecular Devices). The "expose out" signal of the CoolSnap camera was also recorded to synchronize the optical transients with the electrical activity.

RESULTS

Ventral root stimulation triggers bursting of disinhibited networks

The isolated mouse spinal cord generates spontaneous and recurrent bursts of discharge that can be recorded from the ventral roots in the presence of bath-applied bicuculline (20–50 μM) and strychnine (1–5 μM). Within 5 min of drug application, a large-amplitude depolarization followed by continuous but irregular bursting was observed in all recorded ventral roots (Fig. 1*A*). Bursts were initiated by a rapid depolarization, followed by a plateau phase with superimposed oscillations and terminated with a slow decay phase. The induced activity consisted of bursts of average duration 5.1 ± 2.5 s recurring every 48.3 ± 12.6 s (92 bursts measured in 5 experiments) and episodes consisting of several of these bursts occurring every 8–10 min (Fig. 1*A*).

A brief train of stimuli applied to a ventral root could entrain the spontaneous bursting in 31/32 isolated neonatal mouse spinal cord preparations (T_{5-7} to cauda equina). Similar findings have been reported by Machacek and Hochman (2006), who also found that ventral root stimulation could entrain disinhibited ventral root bursting in 2/9 neonatal rats older than P9. Within each preparation, we found that not all of the ventral roots could trigger bursting when stimulated. Overall, stimulation of the ventral roots evoked a disinhibited burst or entrained the disinhibited rhythm in 33% of trials (87/263 ventral roots in 31 preparations). L_6 was the most effective root for entraining/evoking disinhibited bursts (51% of cases in 31 preparations). L_3, L_4, and L_5 were successfully stimulated 30% of the time, whereas stimulation of L_1 and L_2 was successful on only 20% of occasions. This distribution is similar to that for the roots whose stimulation evoked locomotor-like activity (Fig. 1*B*, □). We could trigger locomotor-like activity (Fig. 1*D*) in 43% of all tested roots (72/167 ventral roots in 29 preparations) and stimulation of the L_5 and L_6 roots was the most effective (57% of $L_{5/6}$ roots in 29 preparations). For all experiments, we found a correlation of 0.84 between the ventral root distributions for triggering disinhibited bursts and for evoking locomotor-like activity.

Under control conditions, the ventral root stimulus evoked a slow long-latency depolarizing event (↓ Fig. 1*C*) (see also Mentis et al. 2005) with an average latency to peak of 143 ± 39 ms (range: 63–198 ms, 7 experiments) superimposed on a slow tonic depolarization that potentiated with successive stimuli. If stimulation of a particular root evoked these long-latency depolarizing events (Fig. 1*C, top*) and/or locomotor-like activity (Fig. 1*D*) under control conditions, then stimulation of the same root would generally also evoke/entrain bursting in the disinhibited cord (Fig. 1*C, bottom*). Similarly, if the stimulus *did not* evoke a potential under control conditions then it tended to be ineffective for entraining/evoking a burst under inhibitory blockade (observation made on 45/50 ventral roots tested in both conditions, 9 experiments). The long-latency ventral root-evoked potential was abolished in the presence of the inhibitory antagonists bicuculline and strychnine (Fig. 1*C, bottom*). We consider the possible significance of these observations in the discussion.

Entrainment of burst activity in disinhibited cords

To quantify the entrainment of spontaneous bursting in the disinhibited cord, we applied stimulus trains at inter-train intervals ranging from 2.5 to 25 s. As illustrated in Fig. 2*A,* all of the stimuli were able to entrain the bursting in a sequence of 14 stimulus trains at an intertrain interval of 25 s. However, as the interval between successive trains shortened, the probability that each train evoked a burst decreased (Fig. 2*B*). As shown in the lower sequence of Fig. 2*A*, when the trains were applied every 15 s, several of the trains failed to evoke a burst (Fig. 2*A,* △) although every burst *was* evoked by a stimulus train.

For the first stimulus train, the average delay between the last stimulus of the train and the onset of the burst was 152 ± 46 ms (range: 60–226 ms, 5 experiments, 19 values). This delay progressively lengthened for successive stimulus trains (Fig. 2, *C* and *D*). When the interval between the stimulus trains was 25 s, the delay increased by 13 ± 7 ms (4 experiments, 77 values) with each successive stimulus train (Fig. 2*E*). When the intertrain interval was <10 s, the delay increased substantially: 473 ± 283 ms (3 experiments, 9 values) with successive stimulus trains (Fig. 2*E*).

Ventral-root evoked entrainment of disinhibited bursting was maintained in 3/3 reduced preparations containing just seven segments (L_2–S_2 or T_{13}–L_6), in a two-segment piece (L_2—L=3), and in two hemicords containing five to eight segments (L_4–S_2, T_{12}–L_6).

We also found that dorsal root stimulation could entrain the disinhibited bursts with a single stimulus rather than the five used for ventral root (VR)-induced entrainment (see Fig. 4*B*).

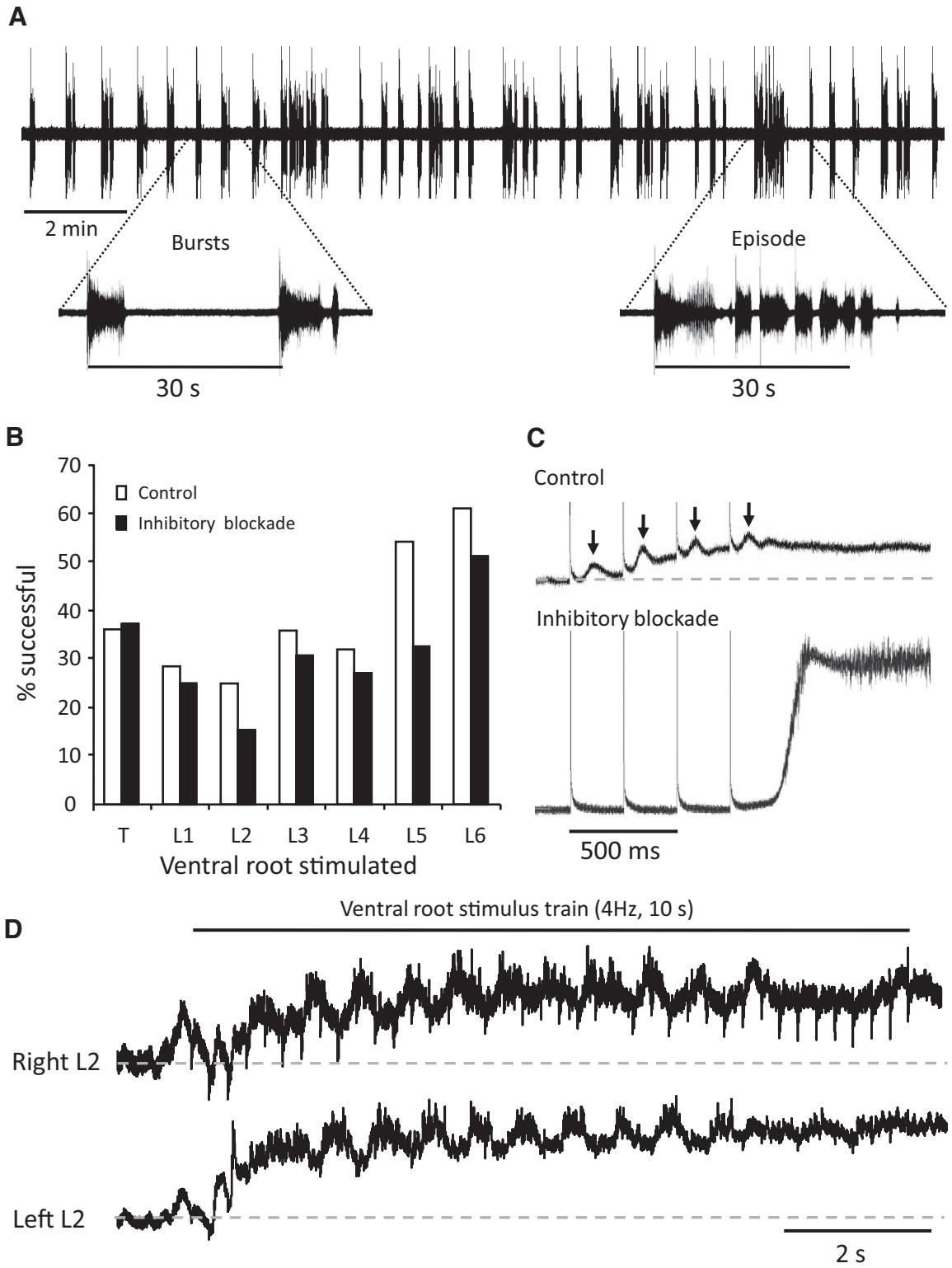

FIG. 1. *A*: spontaneous bursting recorded from the right L_5 ventral root 25 min after application of bicuculline (20 μM) and strychnine (1 μM). *B*: comparison of the percentage of roots from thoracic (T_{11-13}) to L_6 in which stimulation evoked locomotor-like bursting in control (29 experiments) vs. the percentage of roots in which stimulation evoked bursting in the presence of bicuculline and strychnine (31 experiments). *C*: averages of 4 DC recordings of the left L_6 ventral root during 4-Hz trains applied to the left L_5 ventral root (4 stimuli, 50 μA) in control (*top*) and under bicuculline (20 μM) and strychnine (1 μM; *bottom*). Under control conditions, each stimulus of the train evoked a slow long-latency potential ($\downarrow$) superimposed on a tonic depolarization. In the presence of bicuculline and strychnine these potentials were not observed and the stimulus train evoked a burst after a delay. *D*: alternating locomotor-like activity recorded from the left and right L_2 ventral roots and induced by a 4-Hz train, 50 μA applied for 10 s to the left L_5 ventral root (same experiment as in *C*).

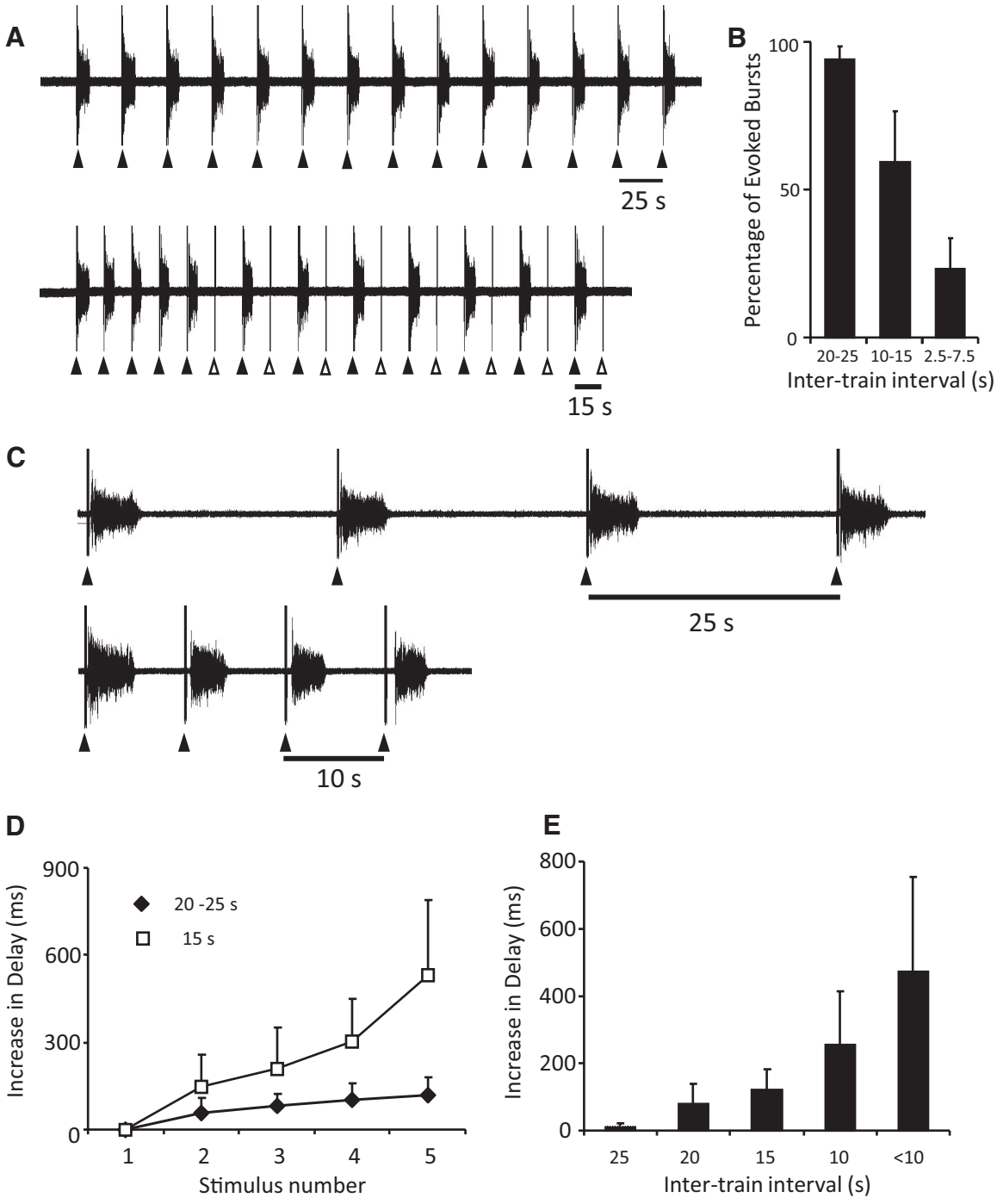

FIG. 2. *A*: in the presence of bicuculline (20 μM) and strychnine (1 μM), bursting on the right L_5 ventral root was entrained by stimulation of the adjacent L_6 ventral root (5 pulses, 4 Hz, 50 μA) every 25 and 15 s. *B*: graph showing the percentage of stimulus trains evoking a burst at different frequencies (8 trains at each frequency $P < 0.0005$, 6 experiments). *C*: the delay between the stimulus train and the onset of a burst increased with successive stimuli and with shorter intertrain intervals. The 1st 4 evoked bursts in a sequence where the intertrain interval was either 25 (*top*) or 10 s (*bottom*). In this experiment, the recording was from the left L_5 ventral root and the adjacent L_6 root was stimulated (bicuculline 20 μM, strychnine 1 μM). *D*: plot of the average increase in the delay (ms) between the last stimulus of the train and the onset of the evoked bursts at 2 different frequencies for 5 consecutive bursts (5 experiments). *E*: plot of the average increase in delay per stimulus for 5 intertrain intervals (4 experiments for 25, 20, and 15 s, 3 experiments for 10 s and <10 s).

In addition, when using dorsal root stimulation, the interval between the stimulus and burst onset was shorter and entrainment could be sustained at higher repetition rates than for VR stimulation. At an intertrain interval of 5 s, the delay between the stimulus and burst onset ranged from 33.9 ± 9.0 ms for the first stimulus to 67.2 ± 26.9 ms for the 10th (4 experiments).

Neurotransmitters involved in mediating the effects of VR stimulation

In the next set of experiments, we investigated the neurotransmitters mediating the entrainment. We first examined the effects of cholinergic blockade on the ability of VR stimulation to entrain the disinhibited rhythm. We found that bath appli-

cation of a mixture of nicotinic (50 μM mecamylamine and 50 μM dihydro-β-erythroidine) and muscarinic (5 μM atropine) antagonists reduced the frequency and duration of spontaneous bursts. Nevertheless, VR entrainment of bursting persisted (6 experiments; Fig. 3*A*) although the delay from the stimulus train to burst onset was increased (Fig. 3*B*). In the presence of bicuculline and strychnine alone, the delay from the last stimulus in the train to the burst onset was 79.1 $\pm$ 11 ms (30 bursts, 3 experiments) and this lengthened to 131.5 $\pm$ 17 ms (28 bursts, 3 experiments) when the cholinergic antagonists were added ($P < 0.05$). The most likely explanation for the increased delay is that the excitability of motoneurons and perhaps other spinal neurons is reduced in the presence of the nicotinic and muscarinic blockers. Indeed it has been shown that local application of the m_2 muscarinic antagonist methoctramine to motoneurons reduces the motoneuronal depolarization accompanying cycles of drug-induced locomotor-like activity in the isolated mouse spinal cord (Miles et al. 2007).

We then investigated the effect of the non-NMDA antagonist NBQX on the ability of VR stimulation to evoke or entrain bursting (7 experiments; NBQX alone, 4 experiments; NBQX and AP5, 2 experiments; NBQX and cyclothiazide, 1 experiment). Bath application of NBQX alone or in the presence of cyclothiazide abolished spontaneous bursting and the ability of VR stimulation to evoke a burst (Fig. 4*A*). Nonetheless, we found that bursting could still be evoked by dorsal root stimulation (Fig. 4*B*) even though all dorsal-root evoked short-latency reflexes were abolished (*C*). Co-application of AP5 and NBQX resulted in the abolition of all spontaneous and evoked bursting (data not shown). In two experiments in which NBQX blocked the VR entrainment, we tried unsuccessfully to evoke bursting, despite the pharmacological blockade, by increasing the stimulus intensity by fivefold.

Collectively, these results suggest that the excitatory effects of VR stimulation on disinhibited bursting require functional glutamatergic neurotransmission. We then investigated the effects of cyclothiazide, a blocker of AMPA receptors desensitization, on the ability of VR stimulation to evoke/entrain disinhibited bursting (Fig. 5). We found that bath-applied cyclothiazide (25 μM) increased both the occurrence of spontaneous bursting and the likelihood of evoking a burst in a sequence of VR stimulus trains. In the presence of cyclothiazide, the average duration of spontaneous bursts decreased from the control value in bicuculline and strychnine of 4.1 $\pm$ 0.4 to 3.3 $\pm$ 0.2 s when cyclothiazide was added (48 bursts, 4 experiments, NS) and the interburst interval fell from 53.4 $\pm$ 5.6 to 16.8 $\pm$ 1.2 s (44 intervals, 4 experiments, $P < 0.0005$). These findings are similar to those reported by Bracci et al. (1996b) in the rat spinal cord. The most likely explanation for the reduced duration is that cyclothiazide increased network excitability resulting in more frequent and secondarily shorter bursts (see Tabak et al. 2001).

Figure 5*A* shows an example of a sequence of 20 stimulus trains (15-s intertrain interval) under control conditions and in the presence of cyclothiazide. Under control conditions 14/20 sequential VR stimuli evoked a burst whereas all 20 stimuli

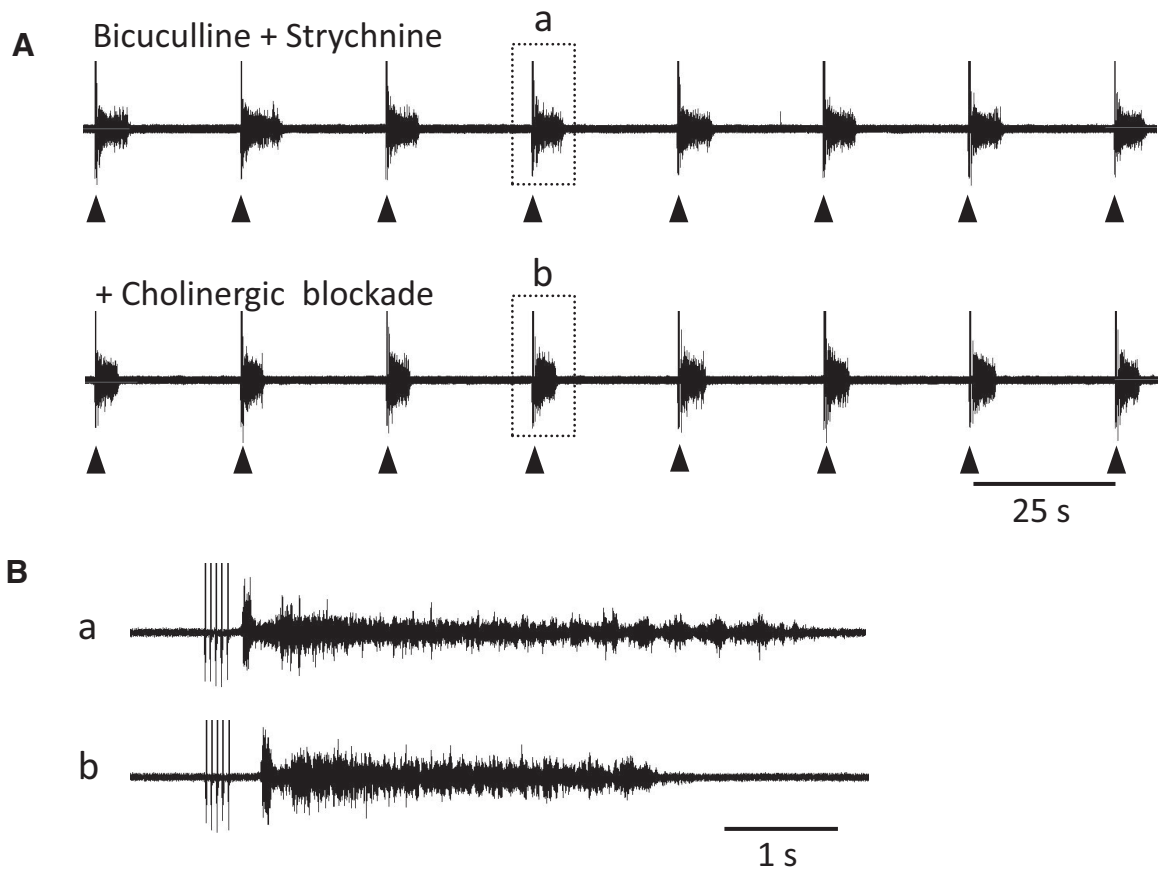

FIG. 3. Entrainment of bursting persists in the presence of cholinergic antagonists. *A*: disinhibited bursting recorded from the left L_6 ventral root is entrained by stimulation (5 pulses, 4 Hz, 50 μA) of the adjacent L_5 ventral root every 25 s (bicuculline 50 μM; strychnine 5 μM). When cholinergic blockers were added to the bath, the entrainment by ventral root stimulation persisted. *B*: the 2 bursts indicated by the boxed areas in *A* (*a* and *b*) displayed at an expanded time scale.

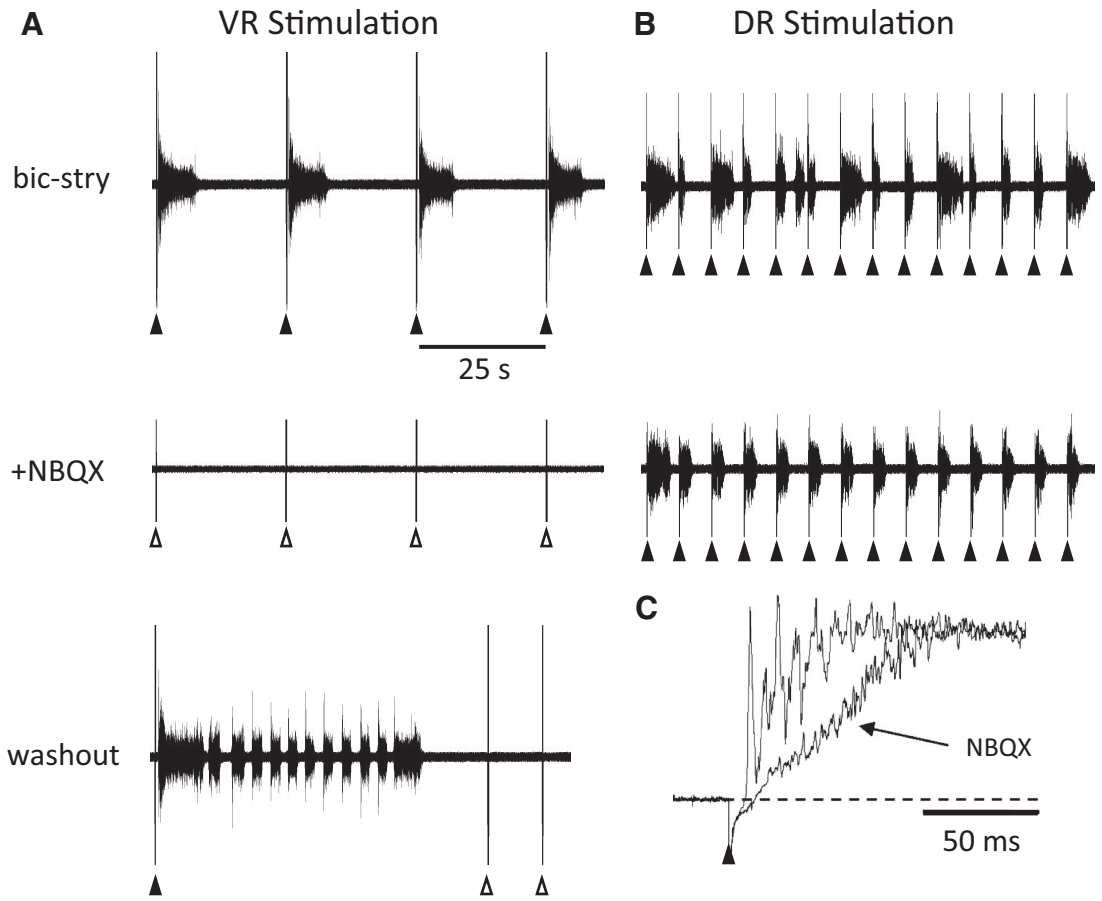

FIG. 4. Entrainment of bursting by ventral but not dorsal root stimulation is abolished by the AMPA receptor antagonist NBQX. *A, top traces*: 4 bursts recorded on the right L_5 ventral root entrained by stimulation (5 pulses, 4 Hz, 60 μA) of the left L_3 ventral root in the presence of bicuculline (20 μM) and strychnine (1 μM). The same trains of stimuli do not evoke bursting 3 min after application of 5 μM NBQX. After washout of the NBQX, bursts were occasionally triggered by ventral root (VR) stimulation. *B*: entrainment of bursting obtained in the same experiment by stimulation of the right L_5 dorsal root (single stimulus, 30 μA) every 5 s. Dorsal root entrainment is maintained 6 min after NBQX application at a time when the ventral root entrainment has been abolished. *C*: in the presence of NBQX, all short-latency L_5 dorsal root-evoked reflexes recorded in the L_5 ventral root are abolished.

were successful in the presence of cyclothiazide. In four experiments of this type (15-s intertrain interval), the number of sequential stimuli that evoked a burst was 6.5 ± 2.5 under control conditions and 11 ± 3.5 in the presence of cyclothiazide ($P < 0.05$).

We also found that the delay between the stimulus and the evoked burst was reduced in the presence of cyclothiazide (Fig. 5*B*). For a sequence of four stimulus trains 15 s apart, the average delay between the train and the onset of the burst was 507.2 ± 160.5 s in the presence of bicuculline and strychnine, and this fell to 133.7 ± 25.9 s when cyclothiazide was added (4 experiments). Figure 5*C* illustrates the progressive increase in the delay for bicuculline/strychnine and in the presence of cyclothiazide. In the presence of bicuculline and strychnine alone, the first delay was 148.2 ± 89.1 s rising to 808.5 ± 595.8 s by the fourth stimulus. When cyclothiazide was added, the values were 67.5 ± 54.3 rising to 188.5 ± 96.1 by the fourth stimulus (4 experiments).

Effects of metabotropic glutamate antagonists on entrained bursting and locomotor-like activity

Previous work has shown that neonatal rodent motoneurons release glutamate or a related amino acid from their synaptic terminals on Renshaw cells (Lamotte d'Incamps and Ascher 2008; Mentis et al. 2005; Nishimaru et al. 2005). If the released excitatory amino acid activated metabotropic glutamate receptors, this might account for the delayed effects of VR stimulation. To test this idea, in three experiments, we examined the effects of antagonists to mGluR1 and mGluR5 on ventral and dorsal root evoked disinhibited bursting and also on locomotor-like activity. We focused on these antagonists because previous work has shown that activation of mGluR1 receptors can accelerate the locomotor rhythm in the lamprey (Krieger et al. 1998) and rat spinal cord (Taccola et al. 2004) and mGluR5 activation slows the locomotor rhythm in the lamprey (Kettunen et al. 2002). In addition, activation of type I mGluRs (mGluR1 and mGluR5) accelerates disinhibited bursting induced by application of bicuculline and strychnine in the neonatal rat cord (Taccola et al. 2004).

We found that the mGluR1 antagonist (CPCCOEt, 80 μM) reduced the ability of a VR train to evoke disinhibited bursts. The effect was particularly marked when short intertrain intervals were used (Fig. 6*A*). In the experiment illustrated, the intertrain interval was 7.5 s for VR stimulation and 5 s for dorsal root stimulation. In the presence of bicuculline and strychnine (control, Fig. 6*A*), the VR stimulus entrained four successive bursts, and in the presence of CPCCOEt, this fell to

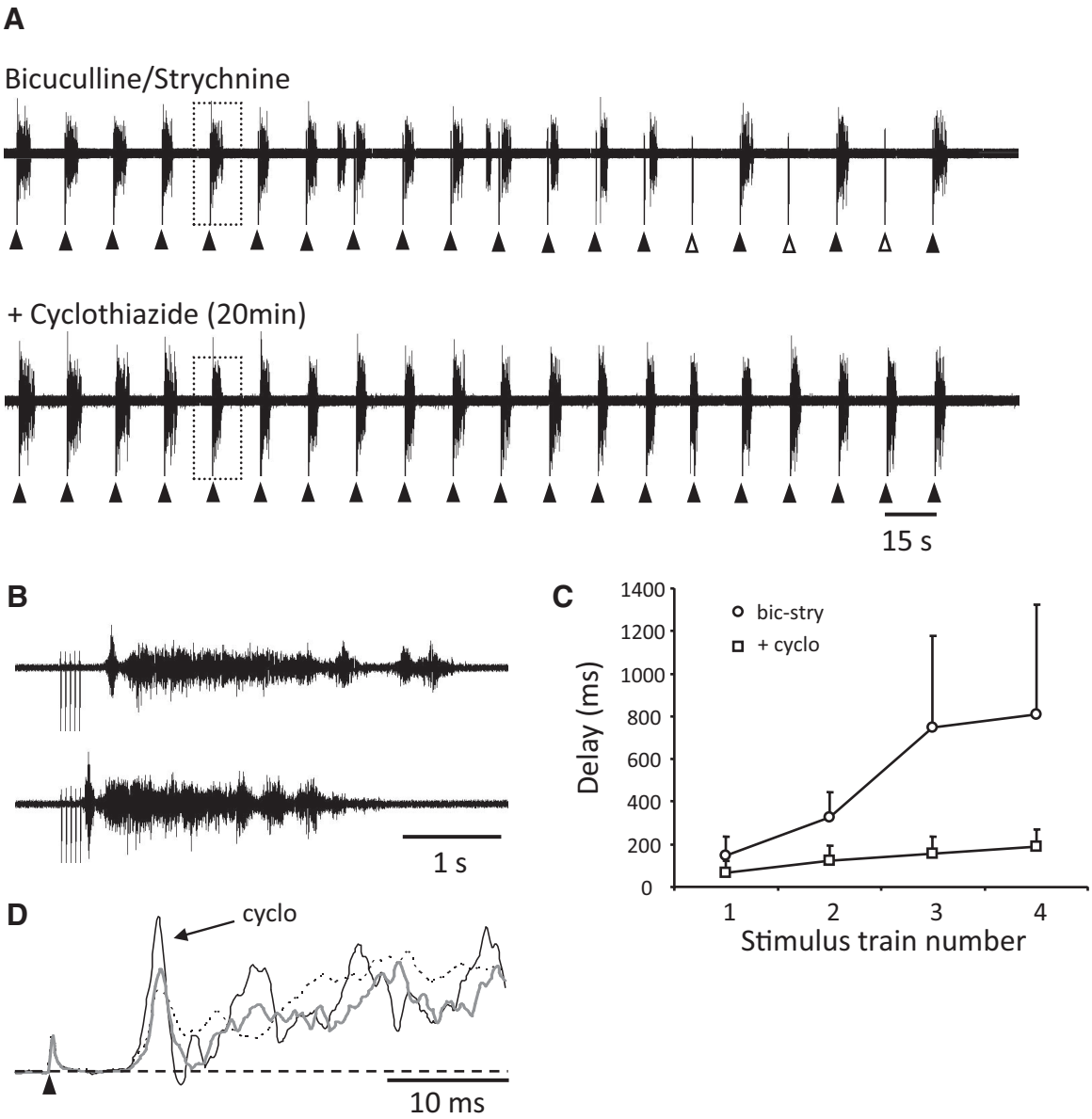

FIG. 5. Entrainment of bursting is more reliable in the presence of the AMPA desensitization blocker cyclothiazide. *A, top trace*: bursts recorded from the right L_5 ventral root in response to stimulus trains (5 pulses, 4 Hz, 25 μA, 200 μs) applied to the right L_6 ventral root every 15 s in the presence of bicuculline (40 μM) and strychnine (4 μM). Note that some of the stimuli do not evoke a burst (open triangles). *Bottom traces*: recordings from the same root in response to the same sequence of stimuli 20 min after application of cyclothiazide (25 μM) showing that each train now evokes a burst. *B*: 2 bursts indicated by the boxed areas in *A* (*a* and *b*) shown at an expanded time scale to illustrate the reduced latency in the presence of cyclothiazide. *C*: graph plotting the average delays between the last stimulus and the onset of the VR-evoked burst for 5 consecutive VR trains applied at a 15-s interval (4 experiments). *D*: records showing the increased amplitude of the monosynaptic reflex recorded from the L_5 ventral root in response to stimulation of the L_5 dorsal root in the presence of cyclothiazide (black trace, cyclo) compared with its amplitude in the presence of bicuculline and strychnine alone (gray trace), and after washout of the cyclothiazide (dotted trace).

a single entrained burst. A similar degradation of entrainment occurred for dorsal root stimulation. To quantify these effects, we compared the number of sequentially entrained bursts for dorsal and VR trains using a 5-s intertrain interval for dorsal root stimulation and a 15-s interval for VR stimulation. When disinhibited bursting was entrained by VR stimulus trains, the number of sequentially entrained bursts was 17.3 $\pm$ 1.2 and this fell to 8.7 $\pm$ 1.3 in the presence of CPCCOEt (80 μM; $P <$ 0.01; 15 entrainment sequences in 3 animals). For dorsal root stimulation in the presence of bicuculline and strychnine, all 20 sequential bursts were entrained. When CPCCOEt (80 μM) was added to the bath, the number fell to 14 $\pm$ 1.8 ($P < 0.01$; 15 entrainment sequences in 3 animals).

The delays from the last stimulus in a VR or a dorsal root train were increased when CPCCOEt was bath-applied. In the presence of bicuculline and strychnine alone, the delay from the last stimulus to the burst onset for the VR-entrained bursts was 55 $\pm$ 0.7 s for the first, rising to 248.3 $\pm$ 48.7 s for the 5th and 131.1 $\pm$ 34 s for the average of the first five bursts. In the presence of CPCCOEt, the delays lengthened to 68 $\pm$ 3.7 s for the first burst, 404 $\pm$ 62.3 for the fifth, and 234.4 $\pm$ 72.2 s for the first five averaged delays ($P < 0.001$, 75 bursts 3 experi-

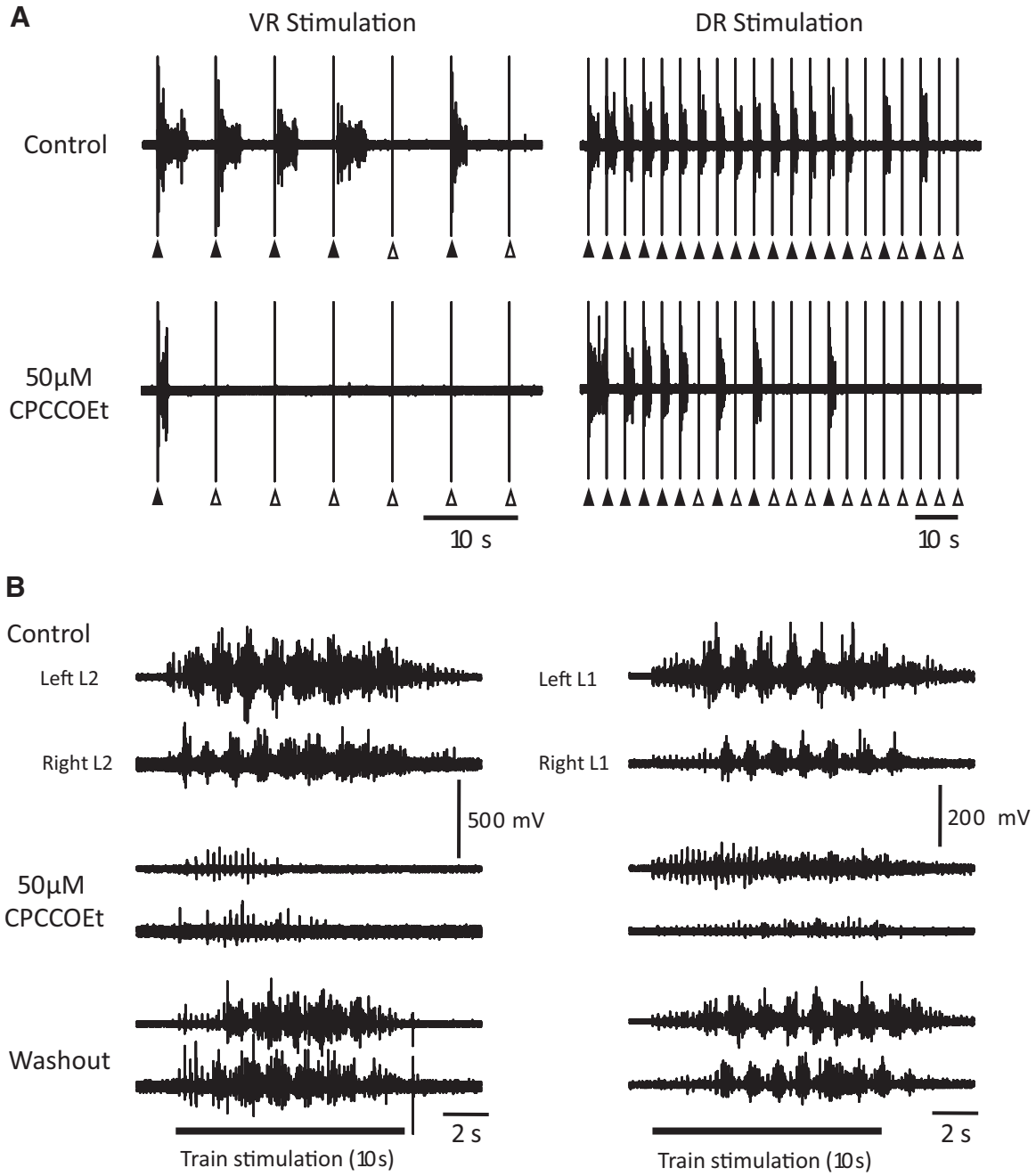

FIG. 6. Entrainment of bursting is less reliable and locomotor-like activity is abolished in the presence of the mGluR1 antagonist 7-(hydroxyimino)cyclopropa[β]chromen-1α-carboxylate ethyl ester (CPCCOEt) *A*: entrainment of bursting in bicuculline and strychnine is less effective in the presence of the mGluR1 antagonist CPCCOEt (50 μM) for both ventral (*left*, VR stimulation) and dorsal (*right*, DR stimulation) stimuli. The interval between the VR stimulus trains (5 stim at 20 Hz; only the last stimulus of the train is shown on the trace) was 7.5 s and between the DR stimuli was 5 s. The DR stimulus intensity was set just below the stimulus intensity to produce 100% entrainment, and resulted in some failures. *B*: CPCCOEt (50 μM) reversibly abolished locomotor-like activity evoked either by a train of ventral root stimuli (*left,* VR stimulation) or dorsal root stimuli (*right,* DR stimulation). Both stimulus trains were 4 Hz for 10 s and are shown by the bar (train stimulation) under the traces.

ments). A similar pattern was found for the DR-evoked bursts. The corresponding delays were 47.6 $\pm$ 1.2 s for the first burst, 73.4 $\pm$ 2.8 s for the fifth, and 65.5 $\pm$ 4.9 s for the average of the first five bursts. In the presence of CPCCOEt, this became 50.5 $\pm$ 1.6 s for the first burst, 99.1 $\pm$ 8.9 for the fifth and 82.54 $\pm$ 8.4 s for the first 5 averaged delays ($P < 0.001$, 75 bursts 3 experiments).

In three experiments, bath-applied CPCCOEt reversibly abolished locomotor-like activity triggered by a 10-s, 4-Hz train of stimuli applied either to the ventral or to the dorsal roots (Fig. 6*B*). Collectively, these results indicate that endogenous activation of mGluR1 receptors is important for the entrainment of disinhibited bursting and appears to be critical for the expression of locomotor-like activity by ventral and dorsal root stimulation.

We also examined the effects of the mGlur5 antagonist (MPEP, 25–50 μM) on the entrained bursting and on locomotor-like activity evoked by dorsal or VR stimulation. We found

little effect of MPEP on the entrained bursting for either dorsal or VR evoked bursting although the amplitude of locomotor-like bursting activity was enhanced in the presence of the drug. These results were not quantified further.

Visualization of neuronal population activity during the initiation of spontaneous or evoked bursting

In the next set of experiments, we used calcium imaging to identify the sequence of recruitment of the neuronal populations activated by the VR stimulus and during spontaneous bursting. This approach has been used successfully to identify a population of Renshaw-like neurons in the chick embryo spinal cord (Wenner and O'Donovan 1999). In the present work, we were particularly interested in the presence of any optical activity during the delay between the VR stimulus and the onset of bursting that might reflect an activated population. We employed two approaches to visualize the activity. In the first, spinal neurons were filled with a calcium sensitive dye by electroporation (see METHODS) (Bonnot et al. 2005) and were imaged through the lateral side of the cord; in the second we used bulk loading of the cut transverse face of the spinal cord to image the caudal end of L_5.

Imaging through the lateral surface of the cord

We imaged optical activity through the lateral aspect of the cord in 16 experiments in which spinal neurons were filled with calcium green dextran by electroporation (Fig. 7*A*). After the experiment, some of the cords were fixed to reveal the extent of labeling and the degree of motoneuron labeling. As illustrated in Fig. 7, electroporation results in extensive labeling of both motoneurons and spinal interneurons. Motoneuronal labeling was confirmed by retrogradely labeling motoneurons with Texas red dextran and establishing the presence of double labeling with the calcium dye and the retrograde tracer (Fig. 7, *B* and *C*) (Bonnot et al. 2005). In addition, in three experiments, antidromic activation of motoneurons was demonstrated optically. The approximate plane of the imaging is shown by the red dotted line in *B*.

We first compared the optical signals generated in response to antidromic stimulation of motoneurons with those accompanying the onset of a burst triggered by the VR stimulus. In contrast to our earlier experiments using retrograde loading of motoneurons (Bonnot et al. 2002), we were not always able to antidromically activate motoneurons by VR stimulation. This may be because the VRs were sometimes damaged during the electroporation process due to their proximity to the electroporation electrodes. However, in three experiments, we were able to show that a part of the ventral optical signal resulted from the activation of motoneurons (Fig. 8).

As illustrated in Fig. 8*A*, antidromic stimulation resulted in a frequency-dependent increase in the fluorescence from the ventral part of the cord. The transients measured at the different frequencies are characteristic of those generated by antidromic stimulation of retrogradely labeled motoneurons (Bonnot et al. 2002). In the presence of bicuculline and strychnine, an antidromic train could trigger a burst as shown in Fig. 8*B*, which allowed regions activated under the two conditions to be compared.

We found that the earliest and strongest optical signals corresponded to the location of motoneurons as identified by antidromic stimulation under control conditions (see Fig. 8*A*), indicating that a significant component of the ventral signal is derived from motoneurons. In this example, the optical activity in the dorsal region began before that in the medial region (see green and red traces in Fig. 8*B, left*). This may be because the VR was stimulated continuously for 2 s rather than with the brief train used for entrainment.

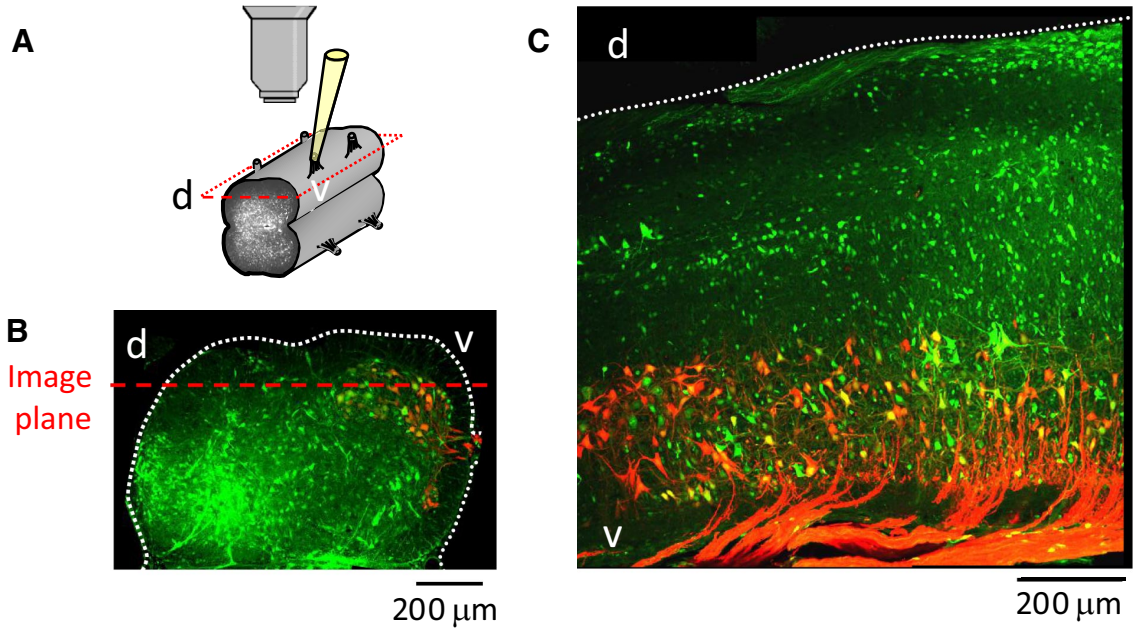

FIG. 7. Arrangement for viewing electroporated cords through the lateral side. *A*: schematic illustrating relationship between objective and cord. *B* and *C*: confocal micrographs of a transverse section of the L_5 segment (*B*) and a parasagittal section ~200 μm from the lateral surface of the L_5 and L_6 segments (*C*) from cords that had been electroporated with the calcium green salt and in which motoneurons were retrogradely labeled with Texas Red Dextran. The dotted red line in *B* shows the approximate plane of view in which motoneurons and laterally situated interneurons were visualized. Confocal images are stacks of ~20 slices taken at 2 μm intervals using a ×20 objective. d-dorsal; v-ventral.

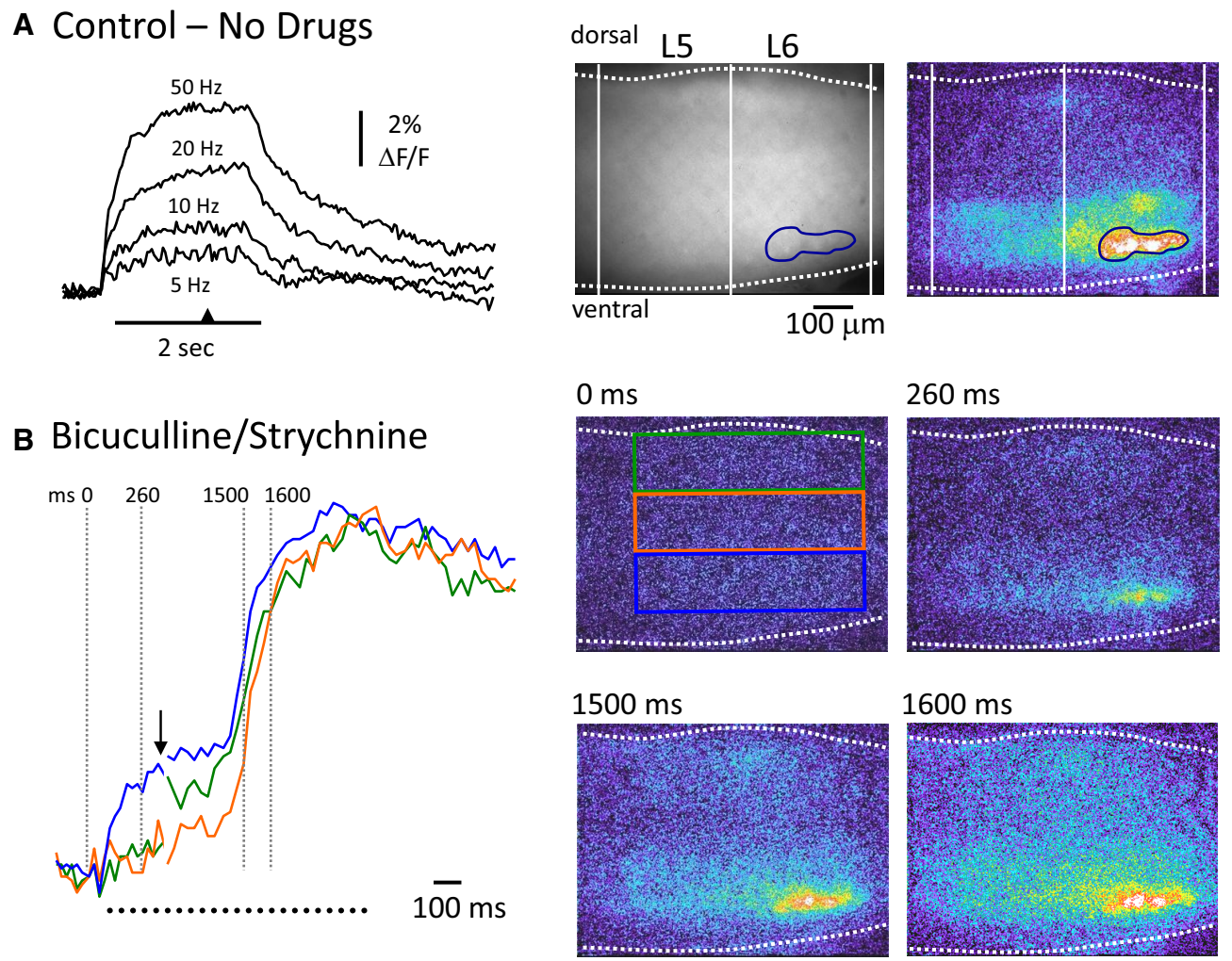

FIG. 8. Comparison of the location of antidromically activated motoneurons and ventrally derived optical signals at the onset of a burst triggered by ventral root stimulation. *A*: antidromic stimulation of motoneurons in the absence of any drugs. *Left*: the fluorescence transients generated from motoneurons (over the area indicated by the blue region of interest shown in the upper 2 video-micrographs to the right) in response to antidromic stimulation of the right L_5 and L_6 ventral roots at several frequencies (indicated above traces). The 1st micrograph in *A*, shows the right L_5–L_6 area of the electroporated cord viewed from the lateral side. *Rightmost*: a difference image (8 frame average) of the fluorescence change in response to 50-Hz stimulation taken at the time indicated by the arrowhead on the time calibration bar in *A*. *B*: a train of stimuli (100 pulses at 50 Hz) applied to the right L_5 and L_6 ventral roots (2 s stimulation) in the presence of bicuculline (40 μM) and strychnine (4 μM) initially antidromically activated motoneurons and then triggered a burst. *Left*: the normalized fluorescence transients recorded from the 3 rectangular regions shown in the videomicrograph at 0 ms. Note that the traces are interrupted at the arrow to show the timing of the activity during the burst in more detail. After the initial antidromic response, a burst is triggered with activity in the ventral region (blue rectangle) leading the activity in the intermediate and dorsal regions. The timing of the last frame in each of the videomicrograph 4 frame averages is shown in milliseconds above the images and over the dotted lines on the fluorescence transients. Each difference image has been subtracted from the prestimulus control and median filtered.

We then quantified the timing and spatiotemporal organization of optical activity accompanying VR evoked bursting (3 experiments), spontaneous bursting (5 experiments), and dorsal root evoked bursting (6 experiments). We measured the activity in a grid comprising six regions of interest spanning the lateral aspect of the spinal cord as shown in Fig. 9*E*. For each region, we calculated the onset time and the time to reach 50% amplitude of the normalized peak (Fig. 9; see METHODS).

The optical activity accompanying a VR stimulus appeared first in the ventral part of the cord and then spread dorsally (Fig. 9*A*). The onset time of the transient in the most dorsal region (dorsal, Fig. 9*E*) was 0.75 ± 0.35 frames or ~25 ms after the onset of the most ventral transient. Given that the distance between the most ventral region and the dorsal region was ~700 μm this corresponds to a propagation speed of ~28 μm/ms. Spontaneously occurring bursts also began ventrally and propagated dorsally although at a somewhat slower velocity (Fig. 9*B*). During spontaneous bursts, the onset of activity in region 5 began 2.0 ± 0.69 frames (~67 ms) after the onset of the most ventral activity corresponding to a propagation velocity of ~7 μm/ms. In contrast to the spontaneous and ventral-root-evoked activity, the bursting initiated by dorsal root stimulation originated dorsally and then propagated ventrally. The onset of activity in the most dorsal region (dorsal) started 2.2 ± 1.2 frames (~73 ms) before the onset of the ventral activity corresponding to a propagation velocity of ~10.4 μm/ms.

The rise time of the calcium transients also differed under the three conditions with activity in the most dorsal regions rising more slowly than that of the ventral regions. These data are plotted in Fig. 9*D*. For a VR stimulus, the time to reach

50% peak amplitude was delayed by 4.0 ± 1.3 frames (133.2 ± 43.3 ms) in the most dorsal region when compared with 50% rise time in the most ventral region (Fig. 9*D*). The calcium transients accompanying spontaneous bursts exhibited a similar time course to those evoked by VR stimulation reaching 50% rise time in the most dorsal region 6.2 ± 1.7 frames (206.5 ± 56.6 ms) after the 50% rise time in the most ventral region.

Imaging the onset of activity on the cut transverse face

A major limitation of the lateral imaging experiments was the inability to image neurons in the medial part of the cord. For this reason, in five experiments, we imaged the optical activity accompanying evoked and spontaneous bursting from the cut transverse face of the spinal cord (rostral L_5) after bulk loading the tissue with the calcium-sensitive dye Fluo-3 (see

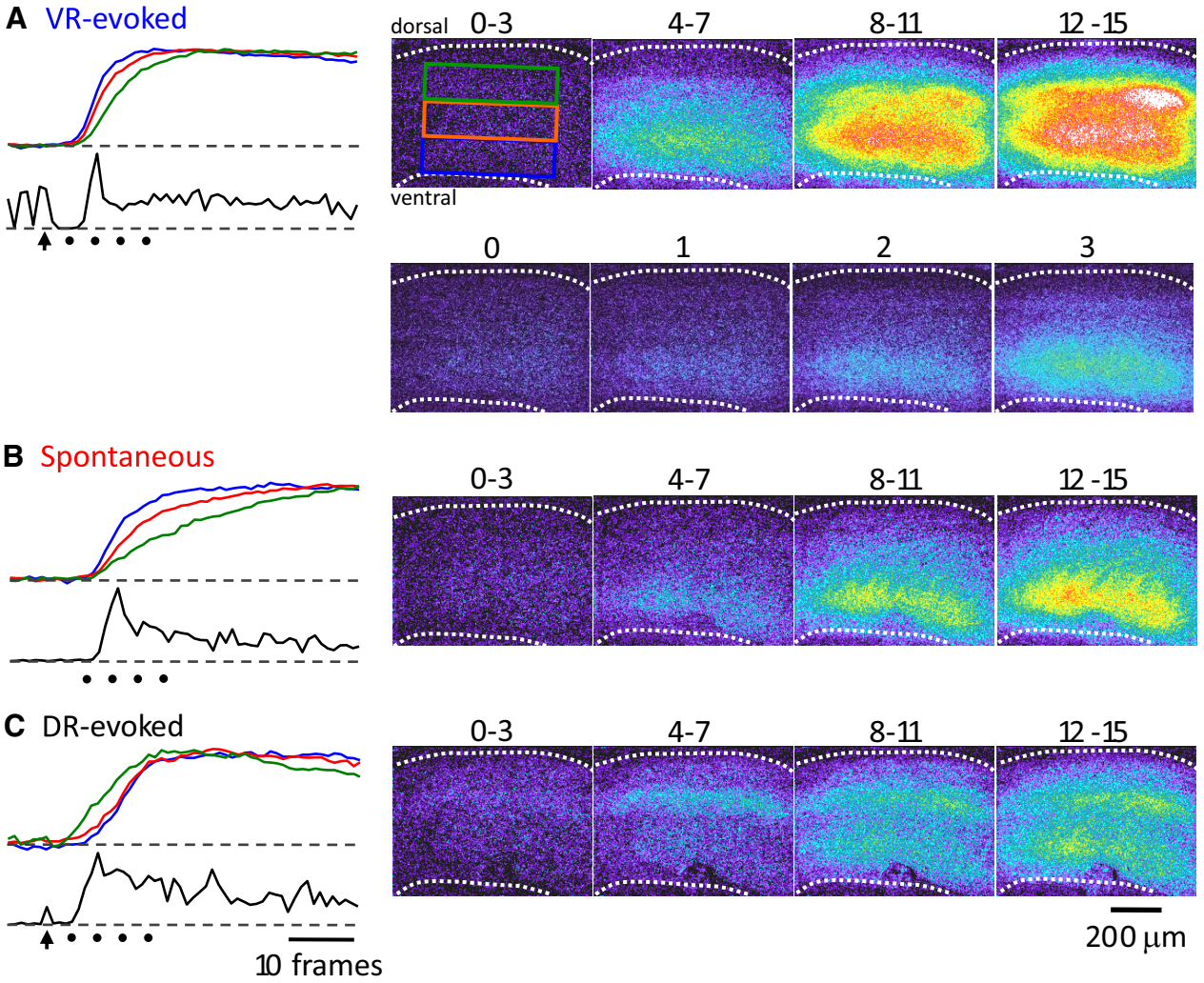

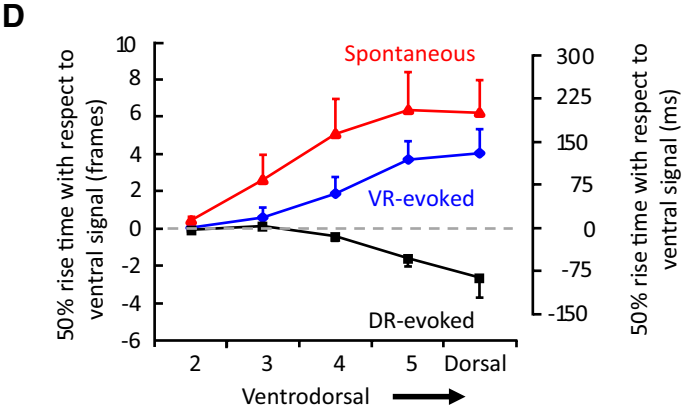

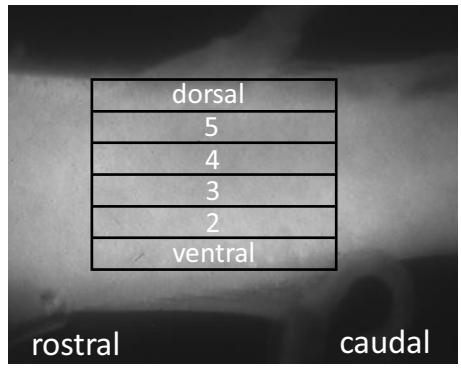

METHODS) (Stosiek et al. 2003; Wilson et al. 2007). Following a VR stimulus, the earliest optical activity originated in the ventrolateral area of the cord and thereafter propagated medially and dorsally (26/26 bursts in 5 experiments; Fig. 10*A*). The antidromic stimuli delivered to the ventral root did not themselves produce a calcium transient presumably because the motoneuron axons closest to the cut face were damaged. However, the surface motoneurons would still be capable of being recruited during the burst and could contribute to the ventral optical signals. Following a dorsal root stimulus, optical activity began in the dorsomedial area of the gray matter and then propagated laterally and ventrally to reach the ventral horn (26/26 bursts in 5 experiments; Fig. 10*C*). The origin of spontaneous activity was more variable. For the majority of spontaneous bursts (26/28, 5 experiments), the optical activity began in the ventral part of the cord (Fig. 10*B*). Of these ventrally originating bursts, in 11/26 the optical activity began in the ventrolateral part of the cord in a similar region to the earliest activity induced by VR stimulation. However, in 12/26 spontaneously occurring bursts, activity began in the ventromedial area and in 3/26 in a region encompassing the complete mediolateral extent of the ventral cord (Fig. 10*B*). In two spontaneous bursts the optical activity originated dorsally.

As was done for the laterally imaged data, we quantified the time to reach 50% amplitude for transients recorded in all five ventrodorsal areas with respect to the time of occurrence of the 50% amplitude of the most ventral transient (Fig. 10, *D* and *E*). Following a VR stimulus the 50% rise time for the transient in the most dorsal part of the cord, occurred 3.21 ± 0.25 frames (67.4 ± 5.3 ms; 30 bursts in 5 experiments) after that of the most ventral transient. The rise time of spontaneously occurring signals was slower than that of the VR-evoked bursts. The 50% amplitude of the optical signal in the most dorsal region occurred 5.65 ± 0.72 frames (118.65 ± 15.12 ms; 30 bursts in 5 experiments) after that of the most ventral transient. The rise time of the dorsal root evoked transients was similar in the three most ventral regions (Fig. 10, *C* and *D*). The 50% rise time for the transient in the most dorsal region occurred 0.86 ± 0.47 frames (18.6 ± 9.9 ms) frames *before* that of the three most ventral regions.

DISCUSSION

In this paper, we have shown that the disinhibited rhythm generated by the lumbosacral cord of the neonatal mouse can be triggered and entrained by a brief train of stimuli applied to a VR. This effect did not require functional cholinergic synaptic connections and was abolished by AMPA/Kainate receptor antagonists. In addition, we have demonstrated that the mGluR1 antagonist CPCCOEt degraded the entrainment of disinhibited bursting by dorsal and VR stimulation and abolished the ability of dorsal and VR stimulation to evoke locomotor-like activity. Calcium imaging of spinal neurons visualized through the lateral aspect of the cord showed that a VR stimulus led to an initial recruitment of ventrally located neurons followed by activation of more dorsal neurons. Imaging in the transverse plane confirmed these findings and revealed that a VR stimulus initiated activity in the ventrolateral part of the cord, suggesting that the neurons synaptically activated by the motoneuron stimulus are located in this region.

Mode of activation of spinal networks by VR stimulation

Although GABA and glycine can be depolarizing in the early neonatal period (Stein et al. 2004; see also Delpy et al. 2008), we can exclude the activation of the network by Renshaw cells because in our study, their synaptic output was blocked by strychnine and bicuculline. An alternative possibility is that the network is activated by a nonspecific effect of motoneuron stimulation—for example potassium release from antidromically activated motoneurons. Indeed an increase in extracellular K^+ has been reported to accompany dorsal root afferent stimulation in the rat spinal cord (Marchetti et al. 2001), which could trigger network activation or lead to the firing of sensory afferents (Kremer and Lev-Tov 1998). We think this explanation for our findings is unlikely. First, the ability of VR stimulation to entrain the disinhibited rhythm was abolished in the presence of the AMPA/kainate receptor blocker NBQX. In itself, this result would not be conclusive because NBQX could block the bursting interneuronal network downstream from the motoneuron-interneuron synapses. However, we could still trigger disinhibited network bursting by dorsal root stimulation in the presence of NBQX, indicating that AMPA/kainate receptors were not essential for network bursting. Furthermore, the ability to entrain bursting was reduced in the presence of the mGluR1 antagonists, suggesting also that K^+ release was not the mechanism.

The possibility that VR stimulation might activate sensory afferents, which in turn would entrain the rhythm is also unlikely because NBQX blocked VR entrainment but not dorsal root entrainment. In addition, in two experiments, we anterogradely loaded the dorsal roots with a calcium-sensitive dye and observed no optical signal following homonymous VR stimulation, while dorsal root stimulation did produce a large optical signal (data not shown).

Entrainment and triggering of disinhibited burst activity by VR stimulation was degraded by mGluR1 antagonism, abolished by NBQX, and enhanced by bath application of the

FIG. 9. Visualization of the spread of optical activity during evoked and spontaneous bursts viewed through the lateral aspect of the cord. *A*—*C*: imaging of an electroporated cord during VR-evoked (*A*), spontaneous (*B*), and DR-evoked (*C*) bursting in the presence of bicuculline (40 μM) and strychnine (4 μM). Each image is a median filtered, 4 frame average of the difference image obtained by subtracting the active frames from a preburst average. The time over the images indicates the frames used in the average. The panels to the *left* of each series of video-micrographs show the optical signals normalized to the peak activity from the ventral (blue), medial (orange), and dorsal (green) areas of the cord (T_{13}–L_1 area, left side) over a 55-frame period (30-Hz acquisition) aligned with the VR activity (black traces under optical signals; left L_6 ventral root in *B* and *C,* and the left L_3 in *A*). The time of the last stimulus in the ventral root train applied to the left T_{13} ventral root (5 pulses, 20 Hz, 55 μA) is shown by the arrow beneath the electrical trace. The arrow in *C* indicates the time of a single stimulus applied to the left T_{13} and L_1 dorsal roots (30 μA). The dots under the electrical traces indicate the timing of the last frame of the 4 frame average for each of the 4 sequential video-micrograph averages shown on the *right*. The frames shown below the images in *A* and marked 0–3 show individual, sequential frames at the onset of the earliest optical activity in response to a ventral root train of stimuli. Each frame has been averaged from video sequences obtained in 4 different ventral-root evoked bursts and shows the ventral origin of the optical activity. *D*: graph summarizing the timing (in frames and in ms) of the fluorescent transients recorded from the regions of interest shown in *E.* The 50% rise time of the optical transient is expressed with respect to the 50% rise time of the most ventral transient. Data are averaged from 5 experiments and expressed as means ± SE.

AMPA receptor desensitization blocker cyclothiazide. Collectively, these results implicate both ionotropic and metabotropic glutamatergic transmission in either the initiation of network activity by VR stimulation, the production of bursts by the network or both.

Previous work has provided evidence that glutamate or a related amino acid is released from motoneuron recurrent collaterals on Renshaw cells (Lamotte d'Incamps and Ascher 2008; Mentis et al. 2005; Nishimaru et al. 2005). However, because the output of Renshaw cells was blocked by bicuccu-

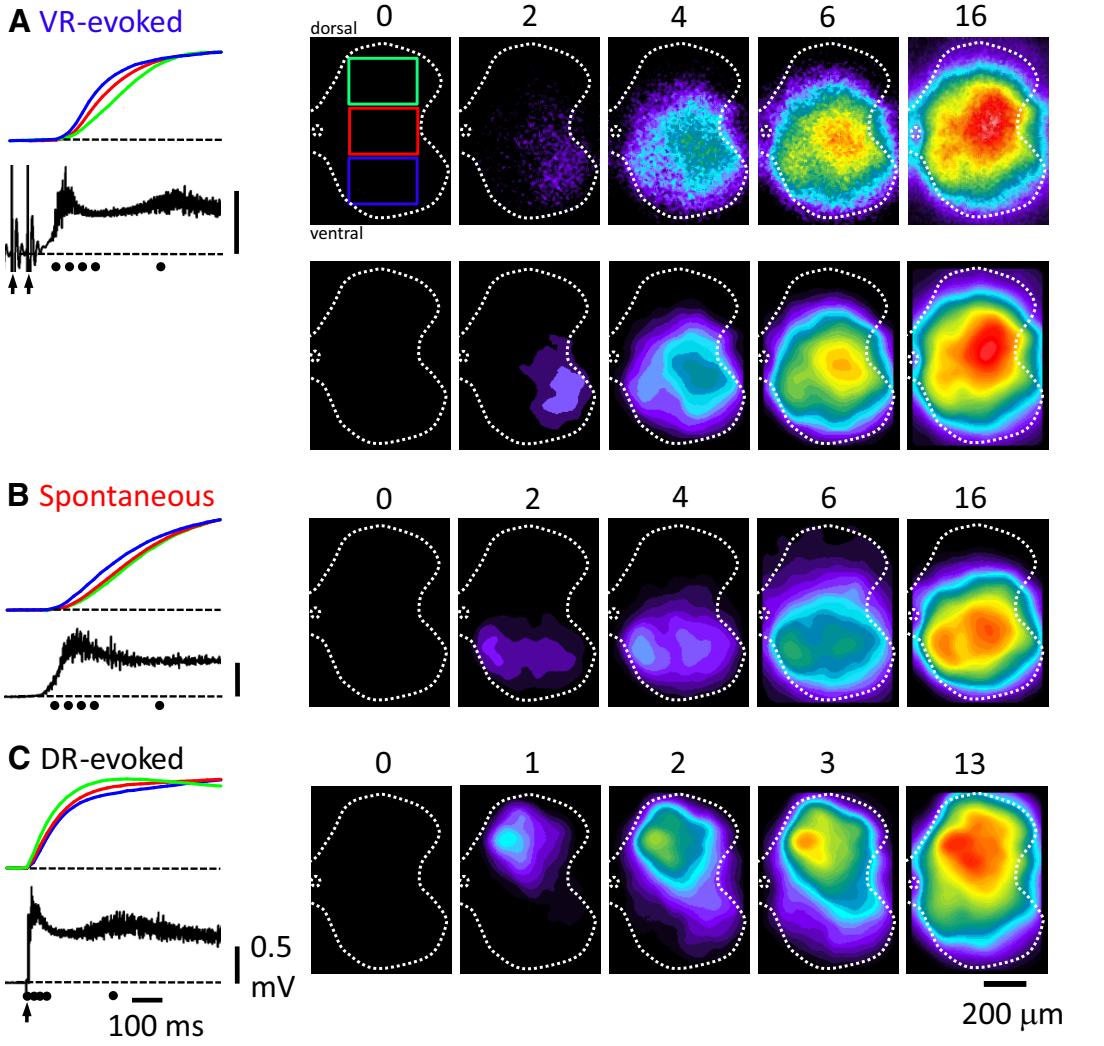

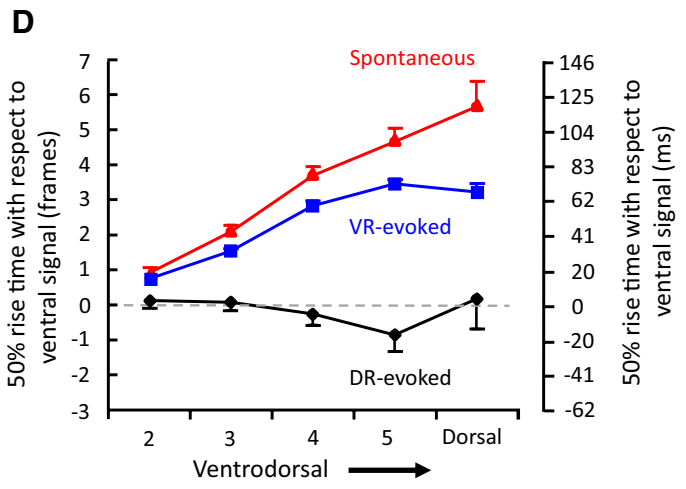

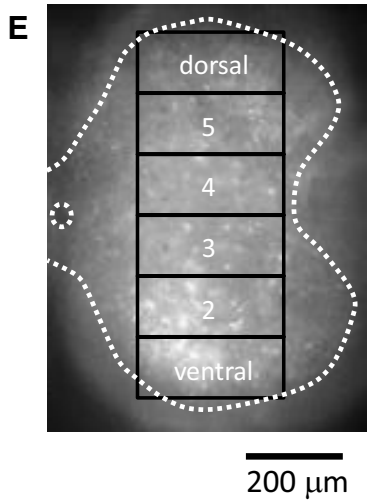

line and strychnine, activation of these synapses cannot mediate the effects of VR stimulation on entrainment. As we discussed in the earlier report (Mentis et al. 2005), it is unlikely that the effects of VR stimulation are mediated through activation of unmyelinated glutamatergic afferents running in the VRs. Although some early reports described the presence of such VR afferents (Coggeshall 1980), more recent work has suggested that if such afferents are present they do not enter the gray matter (Hildebrand et al. 1997; Karlsson et al. 1998). This raises the possibility that motoneurons make glutamatergic synapses with a class of excitatory interneuron in the neonatal mouse spinal cord. This idea is consistent with the results of Machacek and Hochman (2006), who also proposed that a class of excitatory interneurons receive input from motoneurons. From the imaging experiments, we can conclude that the putative interneurons are located in the ventrolateral part of the spinal cord because this is where the initial optical activity occurred during VR stimulation.

Machacek and Hochman (2006) argued that this excitatory pathway was state dependent and could be facilitated or unmasked by noradrenaline. This may account for the lability and variability of the effects of motoneuron stimulation on entrainment in the disinhibited cord and on locomotor-like activity. We noticed that successful activation of the locomotor network by VR stimulation occurred on VRs the stimulation of which evoked a long-latency synaptic potential in the adjacent roots (see Fig. 1*B,* control). We do not know the origin of this potential but note that it disappeared in the presence of bicuculline and strychnine. It is unlikely that this is a depolarizing GABA/glycinergic potential, however, because the equilibrium potential for chloride is known to be either at or below the resting membrane potential in neonatal mouse motoneurons (Delpy et al. 2008). It is possible that the potential reflects the recruitment, under control conditions, of a labile excitatory circuit similar to that described by Machacek and Hochman (2006) in the rat spinal cord, but that is apparently not active in disinhibited bursting.

This hypothesized state-dependence of excitatory pathways activated by motoneuron stimulation may also account for the rostrocaudal differences in the ability of different VRs to entrain the rhythm and to generate locomotor-like activity. Stimulation of L_6 entrained bursting in ~50% of the experiments, whereas L_2 produced entrainment in only ~15% of trials. These differences do not appear to be related to the number of motoneuron axons exiting the VRs. In the adult mouse, the greatest number of myelinated axons are found in L_3 and L_4 VRs (Biscoe et al. 1982), which are among the least effective at activating locomotor-like activity or entraining the disinhibited rhythm. The correlation with unmyelinated fibers is also poor. Biscoe et al. (1982) found that the fewest unmyelinated axons were located in L_2–L_4, which contained on average 19–20 unmyelinated axons in each root. However, the ability to entrain the rhythm or evoke locomotor-like activity was higher in L_3 than in L_1 despite the fact that L_1 contained ~15 times as many unmyelinated axons as L_3.

These rostrocaudal variations in efficacy seem unlikely to be related to size differences of the segments. It might be anticipated that the smaller segments would be better oxygenated and therefore more effective than a larger segment when the corresponding VR was stimulated. However, this did not appear to be true. For instance, L_5, which is one of the largest segments in the lumbar cord, was more effective at evoking both locomotor-like activity and entraining disinhibited rhythms than the much smaller L_2 segment. The absence of a size-related association is consistent with observations in the rat by Machacek and Hochman (2006) who were only able to entrain activity after P9 when the cord is much larger than at earlier ages.

This leaves either some unknown interneuronal specialization along the rostrocaudal axis or some other regionally specialized aspect of spinal cord network organization. In future experiments, it will be necessary to identify the conditions that facilitate expression of these excitatory pathways and to identify the excitatory interneurons responsible for these effects.

Differences between dorsal root and VR entrainment

Stimulation of the dorsal roots was significantly more effective than stimulation of VRs in entraining the disinhibited rhythm or triggering locomotor-like activity. Furthermore, whereas stimulation of any dorsal root along the rostrocaudal extent of the lumbar cord resulted in entrainment, the efficacy of VR stimulation varied rostrocaudally. We have discussed the possible state dependence of excitatory pathways excited by motoneuron stimulation. Another explanation for the difference between ventral and dorsal root stimulation is that many more dorsal root fibers are stimulated than VR fibers. Motoneuron axons are the only known source of excitatory amino acid release in response to VR stimulation and these are substantially outnumbered by glutamatergic afferents in the dorsal roots. In the adult mouse, myelinated dorsal root afferents outnumber myelinated VR fibers by 2–5.5 times, depending on the root (Biscoe et al. 1982). The discrepancy is even more marked for unmyelinated axons; unmyelinated dorsal root axons outnumber VR axons by 10- to 500-fold (Biscoe et al. 1982). Of course, at the stimulus intensities used in our experiments we will not recruit the smallest axons. Nevertheless it is clear that many more dorsal root axons will be stimulated than VR axons.

FIG. 10. Visualization of the spread of optical activity during evoked and spontaneous bursts imaged from the cut transverse face of the rostral L_5 segment. *A–C*: imaging of the fluo-3 AM labeled cord during VR-evoked (*A*), spontaneous (*B*), and DR-evoked (*C*) bursting in the presence of bicuculline (20 μM) and strychnine (5 μM). Each image is a difference image obtained by subtracting a preburst image (average of 5 frames) from the active frames. The top set of images was median filtered and the remaining were rank filtered. The numbers above the images indicate the frames (from stream acquisition performed at 1-ms interframe interval, 20 ms frame duration) selected for illustration. The panels to the *left* show the normalized optical signals from the ventral (blue), medial (red), and dorsal (green) areas of the cord (segment L5, right side) over a 33 frame period aligned with the electrical activity recorded from the ventral root (L_5 in *B* and *C* and L_4 in *A*). The last 2 stimuli of the train applied to the L_5 ventral root (5 pulses, 20 Hz, 200 μs, 80 μA) are shown by the arrows under the electrical trace recorded from L_4 ventral root. The arrow in *C* indicates the time of a single stimulus applied to L_5 dorsal root (200 μs, 25 μA). The dots under the electrical traces indicate the timing of the frame shown on the right. Note in *B* that the spontaneous activity starts ventrally with the major activity ventromedial. *D*: graph summarizing the timing (in frames) of the fluorescent transients measured over 3 regions of interest shown in *E*. The 50% rise time of the optical signal is expressed with respect to the 50% signal rise time in the most ventral area. Data are averaged from 5 experiments and expressed as means ± SE.

Imaging experiments

The earliest detectable optical activity at the onset of a VR-evoked burst occurred in the ventrolateral part of the cord in the region where motoneurons are located. This signal was not due to antidromic activation of motoneurons because it occurred after the stimulus train ended. When we did detect antidromic stimulation of motoneurons optically the signal coincided with the VR stimuli (see Fig. 7*A*). These ventrolaterally originating signals are generated by activity from motoneurons and spinal neurons within or in the vicinity of the motor nucleus. The imaging experiments also revealed that spontaneous activity could also originate in the ventrolateral part of the cord in ~40% of bursts, suggesting that a mechanism similar to that engaged in VR-evoked bursts could be responsible for some spontaneous bursts. However, spontaneous activity could also originate ventromedially (~43% of bursts; Fig. 10*B*), in a region encompassing the complete mediolateral extent of the ventral cord (10% of bursts) or infrequently in the dorsal horn (7% of bursts). The interpretation of the origin of spontaneous bursting is complicated by the fact that the cord was cut to view the transverse face, which may have altered the local pattern of recruitment. However, the lateral imaging was largely consistent with the transverse imaging showing that activity originated in a ventral band spanning several segments rostrocaudally, suggesting that the transverse imaging was accurately reporting the locus of the initial activity.

Comparison with previous studies

In the rat spinal cord, Machacek and Hochman (2006) were able to entrain disinhibited bursting in two of nine experiments on animals aged P11–P14. Entrainment was evoked by a single stimulus and the authors did not report trying other stimulus patterns. Entrainment was unsuccessful on animals <9 days old. In contrast, Bracci et al. (1997) were unable to entrain bursting in the disinhibited cord by either single or multiple stimuli applied to a VR. These experiments were also performed on the neonatal rat but the age of the animals was not documented for those experiments in which VR entrainment was investigated. In the present work, we were able to entrain bursting in 29/30 experiments in animals aged P2–P3. It is not clear what accounts for this difference between mouse and rat.

Significance to studies of locomotion

The mechanism of activation of the locomotor network by VR stimulation is unknown but it shares several features with the entrainment of disinhibited rhythms by VR stimulation. First, the VRs whose stimulation produces either entrainment of disinhibited bursting or locomotion were similar (see Fig. 1*C*). In both situations, the most effective roots were the lower thoracic and the lower lumbar roots. Second, both effects persisted in the presence of cholinergic blockers and were blocked by glutamatergic antagonists. Finally, antagonism of mGluR1 receptors abolished the ability of VR stimulation to evoke locomotor like activity and reduced the efficacy of VR entrainment of disinhibited bursts. These findings suggest a common mode of activation for locomotor and disinhibited networks by VR stimulation and provide additional evidence that motoneurons may play a more active role in locomotor activity that has generally been assumed.

ACKNOWLEDGMENTS

Present address of A. Bonnot, RCCN, Neurobiologie des Processus Adaptatifs, CNRS UMR 7102, Université PM Curie, Paris, France.

GRANTS

This work was supported by the intramural program of the National Institutes of Neurological Disorders and Stroke.

REFERENCES

Arai Y, Mentis GZ, Wu J and O'Donovan MJ. Ventro-lateral origin of activity during each cycle of spontaneous activity generated by the spinal cord of the chick embryo *PLoS ONE* 2: e417, 2007.

Beato M, Bracci E, Nistri A. Contribution of NMDA and non-NMDA glutamate receptors to locomotor pattern generation in the neonatal rat spinal cord. *Proc Biol Sci.* 264: 877–884, 1997.

Beato M, Nistri A. Interaction between disinhibited bursting and fictive locomotor patterns in the rat isolated spinal cord. *J Neurophysiol.* 82: 2029–2038, 1999.

Biscoe TJ, Nickels SM, Stirling CA. Numbers and sizes of nerve fibres in mouse spinal roots. *Q J Exp Physiol* 67: 473–494, 1982.

Bonnot A, Mentis GZ, Skoch J, O'Donovan MJ. Electroporation loading of calcium-sensitive dyes into the central nervous system *J Neurophysiol* 93: 1793–1808, 2005.

Bonnot A, Whelan P, Mentis GZ, O'Donovan MJ. Spatiotemporal pattern of motoneuron activation in the rostral lumbar and sacral segments during locomotor-like activity in the neonatal mouse spinal cord. *J Neurosci* 203: 1–6, 2002.

Bracci E, Ballerini L, Nistri A. Localization of rhythmogenic networks responsible for spontaneous bursts induced by strychnine and bicuculline in the rat isolated spinal cord. *J Neurosci* 16: 7063–7076, 1996a.

Bracci E, Ballerini L, Nistri A. Spontaneous rhythmic bursts induced by pharmacological block of inhibition in lumbar motoneurons of the neonatal rat spinal cord. *J Neurophysiol* 75: 640–647, 1996b.

Bracci E, Beato M, Nistri A. Afferent inputs modulate the activity of a rhythmic burst generator in the rat disinhibited spinal cord in vitro. *J Neurophysiol* 77: 3157–3167, 1997.

Coggeshall RE. Law of separation of function of the spinal roots. *Physiol Rev* 60: 716–755, 1980.

Cowley KC, Schmidt BJ. Effects of inhibitory amino acid antagonists on reciprocal inhibitory interactions during rhythmic motor activity in the in vitro neonatal rat spinal cord. *J Neurophysiol* 74: 1109–1117, 1995.

Delpy A, Allain AE, Meyrand P, Branchereau P. NKCC1 cotransporter inactivation underlies embryonic development of chloride-mediated inhibition in mouse spinal motoneuron. *J Physiol* 586: 1059–1075, 2008.

Hildebrand C, Karlsson M, Risling M. Ganglionic axons in motor roots and pia mater. *Prog Neurobiol* 51: 89–128, 1997.

Jiang ZG, Shen E, Wang MY, Dun NJ. Excitatory postsynaptic potentials evoked by ventral root stimulation in neonate rat motoneurons in vitro. *J Neurophysiol* 65: 57–65, 1991.

Juvin L, Simmers J, Morin D. Propriospinal circuitry underlying interlimb coordination in mammalian quadrupedal locomotion. *J Neurosci* 25: 6025–6035, 2005.

Karlsson M, Zakrisson M. Relation between putative afferent axons and the glia limitans in rat motor roots. *J Peripher Nerv Syst* 3: 47–53, 1998.

Kettunen P, Krieger P, Hess D, El Manira A. Signaling mechanisms of metabotropic glutamate receptor 5 subtype and its endogenous role in a locomotor network. *J Neurosci* 22: 1868–1873, 2002.

Kjaerulff O, Kiehn O. Distribution of networks generating and coordinating locomotor activity in the neonatal rat spinal cord in vitro: a lesion study. *J Neurosci.* 16: 5777–5794, 1996.

Kremer E, Lev-Tov A. GABA-receptor-independent dorsal root afferents depolarization in the neonatal rat spinal cord. *J Neurophysiol* 79: 2581–2592, 1998.

Krieger P, Grillner S, El Manira A. Endogenous activation of metabotropic glutamate receptors contributes to burst frequency regulation in the lamprey locomotor network. *Eur J Neurosci* 10: 3333–3342, 1998.

Lamotte d'Incamps B, Ascher P. Four excitatory postsynaptic ionotropic receptors coactivated at the motoneuron-Renshaw cell synapse. *J Neurosci* 28: 14121–14131, 2008.

Machacek DW, Hochman S. Noradrenaline unmasks novel self-reinforcing motor circuits within the mammalian spinal cord. *J Neurosci* 26: 5920–5928, 2006.

Marchetti C, Beato M, Nistri A. Evidence for increased extracellular $K(^{+})$ as an important mechanism for dorsal root induced alternating rhythmic activity in the neonatal rat spinal cord in vitro. *Neurosci Lett* 304: 77–80, 2001.

Mentis GZ, Alvarez FJ, Bonnot A, Richards DS, Gonzalez-Forero D, Zerda R, O'Donovan MJ. Non-cholinergic excitatory actions of motoneurons in the neonatal mammalian spinal cord. *Proc Natl Acad Sci USA* 102: 7344–7349, 2005.

Miles GB, Hartley R, Todd AJ, Brownstone RM. Spinal cholinergic interneurons regulate the excitability of motoneurons during locomotion. *Proc Natl Acad Sci USA* 104: 2448–2453, 2007.

Nishimaru H, Restrepo CE, Ryge J, Yanagawa Y, Kiehn O. Mammalian motor neurons corelease glutamate and acetylcholine at central synapses. *Proc Natl Acad Sci USA* 102: 5245–5249, 2005.

Perrins R, Roberts A. Cholinergic contribution to excitation in a spinal locomotor central pattern generator in *Xenopus* embryos. *J Neurophysiol* 73: 1013–1019, 1995.

Stein V, Hermans-Borgmeyer I, Jentsch TJ, Hubner CA. Expression of the KCl cotransporter KCC2 parallels neuronal maturation and the emergence of low intracellular chloride. *J Comp Neurol* 468: 57–64, 2004.

Stosiek C, Garaschuk O, Holthoff K, Konnerth A. In vivo two-photon calcium imaging of neuronal networks. *Proc Natl Acad Sci USA* 100: 7319–7324, 2003.

Tabak J, Rinzel J, O'Donovan MJ. The role of activity-dependent network depression in the expression and self-regulation of spontaneous activity in the developing spinal cord of the chick embryo *J Neurosci* 21: 8966–8978, 2001.

Taccola G, Marchetti C, Nistri A. Modulation of rhythmic patterns and cumulative depolarization by group I metabotropic glutamate receptors in the neonatal rat spinal cord in vitro. *Eur J Neurosci* 19: 533–541, 2004.

Wenner P, O'Donovan MJ. Identification of an interneuronal population that mediates recurrent inhibition of motoneurons in the developing spinal cord. *J. Neuroscience* 19: 7557–7567, 1999.

Wenner P, **O'Donovan MJ.** Mechanisms that initiate spontaneous network activity in the developing chick spinal cord. *J Neurophysiol* 86: 1481–1498, 2001.

Wilson JM, Dombeck DA, Dıaz-Rıos M, Harris-Warrick RM, Brownstone RM. Two-photon calcium imaging of network activity in XFP-expressing neurons in the mouse. *J Neurophysiol* 97: 3118–3125, 2007.